

# Terahertz electromagnetic waves emitted from semiconductor investigated using terahertz time domain spectroscopy

(Invited Paper)

Yiming Zhu (朱亦鸣)<sup>1,2\*</sup> and Songlin Zhuang (庄松林)<sup>1</sup>

<sup>1</sup>Engineering Research Center of Optical Instrument and System, Ministry of Education, Shanghai Key Lab of Modern Optical System, University of Shanghai for Science and Technology, Shanghai 200093, China

<sup>2</sup>School of Microelectronics, Shanghai Jiao Tong University, Shanghai 200240, China

\*Corresponding author: ymzhu@usst.edu.cn

Received June 30, 2011; accepted July 28, 2011; posted online September 27, 2011

Ultrafast electromagnetic waves radiated from semiconductor material under high electric fields and photoexcited by femtosecond laser pulses have been recorded by using terahertz time domain spectroscopy (THz-TDS). The waveforms of these electromagnetic waves reflect the dynamics of the photoexcited carriers in the semiconductor material, thus, THz-TDS provides a unique opportunity to observe directly the temporal and spatial evolutions of non-equilibrium transport of carriers within sub-picosecond time scale. We report on the observed THz emission waveforms emitted from GaAs by using a novel technology, the time domain THz electro-optic (EO) sampling, which has a bipolar feature, i.e., an initial positive peak and a subsequent negative dip that arises from its velocity overshoot. The initial positive peak has been interpreted as electron acceleration in the bottom of  $\Gamma$  valley in GaAs, where electrons have a light effective mass. The subsequent negative dip has been attributed to intervalley transfer from  $\Gamma$  to X and L valleys. Furthermore, the power dissipation spectra of the bulk GaAs in THz range are also investigated by using the Fourier transformation of the time domain THz traces. From the power dissipation spectra, the cutoff frequency for negative power dissipation (i.e., gain) under step electric field in the bulk GaAs can also be obtained. The cutoff frequency for the gain gradually increases with increasing electric fields up to 50 kV/cm and achieves saturation at approximately 1 THz at 300 K. Furthermore, based on the temperature dependence of the cutoff frequency, we find that this cutoff frequency is governed by the energy relaxation process of electrons from L to  $\Gamma$  valley via successive optical phonon emission.

OCIS codes: 320.7130, 300.6495, 160.6000.

doi: 10.3788/COL201109.110007.

## 1. Introduction

Ultrafast non-equilibrium transport of carriers in semiconductors biased at high electric fields is of fundamental interest in semiconductor physics. From a fundamental point of view, the detailed understanding of the femtosecond dynamics of carriers in an electric field is a key issue in many body physics. Furthermore, the clarification of carrier dynamics under extreme non-equilibrium conditions is strongly motivated by the need to obtain information relevant to the design of ultrahigh speed devices. Even the use of transit times with less than 1 ps has been reported for compound semiconductor field effect transistors<sup>[1]</sup>. In these ultrashort channel transistors, carriers experience very few scattering events in the channel as well as a drift in a highly non-stationary manner as schematically illustrated in Fig. 1. Consequently, the performance of such ultrafast transistors is not determined mainly by the steady-state properties, such as saturation velocities and mobilities. Performance is governed by the non-stationary carrier transport subjected to high electric fields. Therefore, it is essential to understand non-equilibrium transport of carriers subjected to high electric fields in such devices.

Furthermore, it is well known that in numerous compound semiconductors, such as GaAs, negative

differential conductivities (NDCs) appear under high electric fields due to intervalley transfer. NDCs, which refer to the gain, are of practical importance, notably for their exploitation in microwave and terahertz (THz) wave oscillators<sup>[2]</sup>. However, because NDC gain has a finite bandwidth, it provides an intrinsic upper frequency limit to ultrafast electromagnetic wave oscillators. For this reason, a number of works have investigated the mechanism that limits the bandwidth of the gain. Researchers have found that the mechanism is mainly controlled by the energy relaxation time of electrons<sup>[3–5]</sup>. Monte Carlo results predict that the real part of the negative differential mobility (i.e., gain) can persist up to a few hundred gigahertz. Together with theoretical studies, efforts have been devoted to enhance the high frequency limit and push it into the THz frequency range in real devices. Gunn and IMPATT diodes have already been operated at frequencies of 100–200 GHz<sup>[6–8]</sup>. However, in these experiments, the cutoff operation frequency,  $\nu_c$ , is governed mainly not by the material properties themselves but by electronic circuits, i.e., stray capacitance and inductance, and more fundamentally by the length of the samples. Therefore, in spite of the numerous investigations using a variety of methods<sup>[9–11]</sup>, it is extremely important to characterize the gain bandwidth of materials in the THz range for THz wave generation.

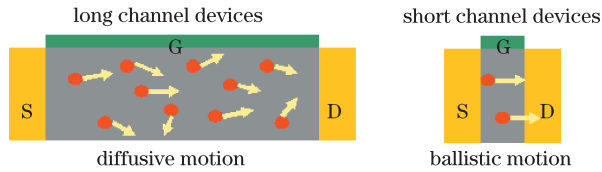


Fig. 1. Carrier transport in (a) long diffusive channels and (b) very short ballistic channels. In conventional long-channel transistors, performance is determined by steady-state properties, such as saturation velocities and mobilities. However, in very short channel transistors, carrier transport is quasi-ballistic and switching speed is governed by the speed with which carriers are accelerated.

Achieving significant results using the conventional method for determining the sub-picosecond non-equilibrium transport of electrons and gain in the THz range is almost impossible for the following reasons. (i) For these measurements, a large sample size, typically a few square millimeters, is necessary. An extremely large current follows through the sample under biased conditions. (ii) To a great extent, the profile of internal electric field in doped GaAs becomes non-uniform due to the formation of high field domains. Thus far, these two inevitable issues have made conventional measurements practically impossible to implement.

THz time domain spectroscopy (THz-TDS) provides a relevant opportunity to observe the motion of electron wave packet in the sub-picosecond time range and to measure inherently the response of the electron system to the applied bias electric field<sup>[12–17]</sup>. Furthermore, the Fourier spectra of the THz emission provide the power dissipation spectra under step electric field in the THz range, from which we can obtain the gain region of the material in the THz range<sup>[16,17]</sup>.

We have investigated the non-equilibrium acceleration of carriers in bulk GaAs subjected to very high electric fields by THz-TDS<sup>[15]</sup>. It was found that THz emission waveforms possess a bipolar feature characterized with an initial positive peak and a subsequent negative dip that results from the velocity overshoot. The initial positive peak has been interpreted as electron acceleration in the bottom of  $\Gamma$  valley in GaAs, where electrons have a light effective mass, whereas the subsequent negative dip has been attributed to the intervalley transfer from  $\Gamma$  to X and L valleys. Furthermore, based on the Fourier transformation of the time domain THz traces, the power dissipation spectra under step electric field in the THz range have been obtained<sup>[16,17]</sup>. The cutoff frequency for negative power dissipation of the bulk GaAs can also be derived from the power dissipation spectra. The cutoff frequency for the gain gradually increases as the electric fields increased up to 50 kV/cm and saturates at approximately 1 THz at 300 K/750 GHz at 10 K. We have also investigated the temperature dependence of the cutoff frequency for negative power dissipation, from which we have determined that the cutoff frequency is governed by the energy relaxation process of electrons from L to  $\Gamma$  valley via successive optical phonon emission.

## 2. Experiments

Undoped bulk GaAs sample grown by molecular beam

epitaxy was used in our experiment. Sample #1 had an  $m-i-n$  geometry with a 1- $\mu\text{m}$ -thick intrinsic GaAs layer, whereas sample #2 had the same structure but with a 180-nm-thick intrinsic GaAs layer. An ohmic contact was fabricated by depositing and annealing AuGeNi alloy on the back side of the sample. A semitransparent NiCr Schottky film was deposited on the surface to apply a direct current (DC) electric field,  $F$ , to the intrinsic GaAs layer. The sample was mounted on a copper plate, which was placed in the cryostat for the THz-TDS measurements. The illuminated surface area (window area) was approximately  $1.5 \times 1$  (mm). The special design of this window size was adopted to avoid the field screening effect.

Femtosecond laser pulses from a mode locked Ti:sapphire laser operated at a repetition rate of 76 MHz was used for THz-TDS. The full-width at half-maximum (FWHM) of the spectral bandwidth of femtosecond laser pulses was approximately 20 meV. The central photon energies of the light pulses were set to 1.422 eV at 300 K and 1.515 eV at 10 K, in a manner by which electrons can be created near the bottom of conduction band and holes can be produced near the top of valence band. Free space electro-optic (EO) sampling technique was used to record the temporal waveforms of the THz electric fields emitted from the samples. This is shown in Fig. 2<sup>[18,19]</sup>. The EO sensor used was a 100- $\mu\text{m}$ -thick (110)-oriented ZnTe crystal. The spectral bandwidth of the sensor was approximately 4 THz<sup>[20,21]</sup>, as shown in Fig. 3.

Figure 4 shows the temporal waveforms of THz electric fields emitted from sample #1 for various  $F$  values of 300 and 10 K (Figs. 4(a) and (b)). In Ref. [22], the

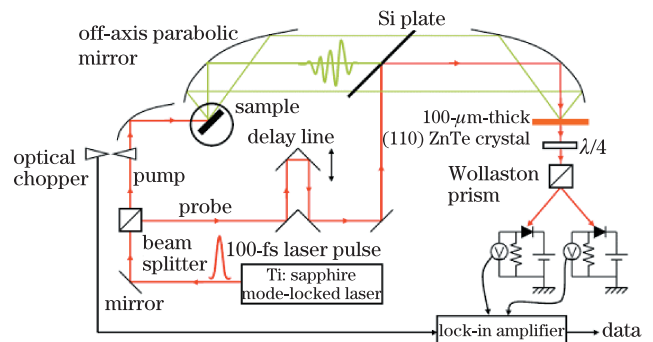


Fig. 2. Experimental setup for free space EO sampling.

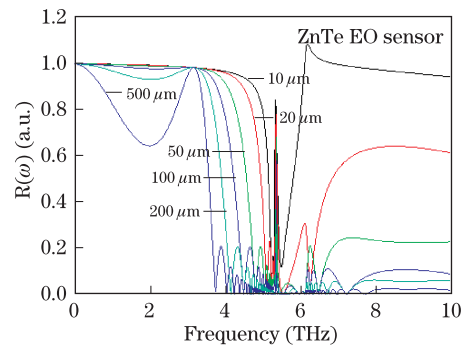


Fig. 3. Calculated amplitude response  $R(\omega)$  of the ZnTe EO sensor with different thicknesses, normalized as unity at low frequencies.

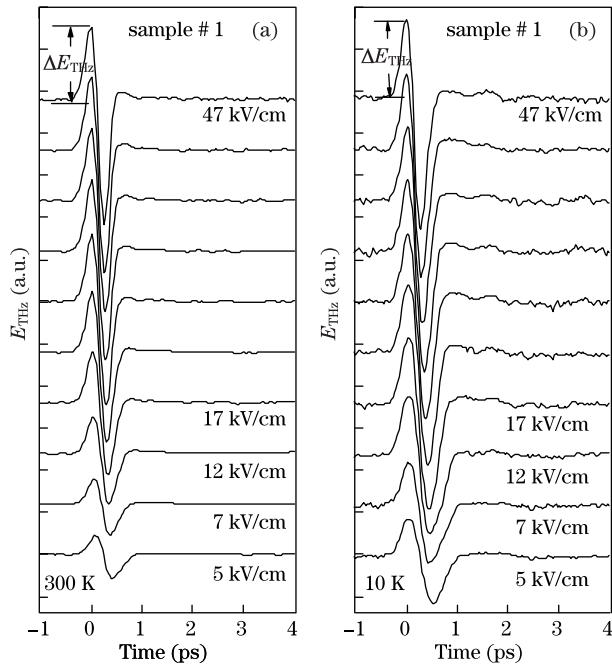


Fig. 4. Bias field dependence of the temporal waveforms of THz electric field ( $E_{\text{THz}}$ ) emitted from sample #1 at (a) 300 and (b) 10 K.

position of  $t = 0$  was determined empirically by choosing a position which did not cause artificial jumps in the phase of the Fourier spectra of (THz-TDS). To determine the position of  $t = 0$  more accurately, we adopted a newly developed method, the maximum entropy method (MEM)<sup>[23–25]</sup>. The position of  $t = 0$  set in Fig. 4 is determined by MEM with an error of  $\pm 30$  fs, which is limited by the time interval of recorded points.

### 3. Discussion

From the Maxwell equations

$$\begin{cases} \nabla \times E = -\mu_0 \frac{\partial H}{\partial t} \\ \nabla \times H = J + \frac{\partial D}{\partial t} \end{cases}, \quad (1)$$

THz electric field,  $E_{\text{THz}}$ , induced by transient current,  $J$ , due to photoexcited carriers is given by

$$E_{\text{THz}} \propto \frac{\partial v}{\partial t}. \quad (2)$$

$E_{\text{THz}}$  is the emitted ultrafast electromagnetic wave, which is proportional to carrier acceleration. The inter-band transitions induced by ultrashort excitation pulses create electrons close to the bottom of  $\Gamma$  valley in the conduction band as well as holes near the top of valence band. In an ideal case without scattering, these electrons are accelerated ballistically by the applied electric field in  $\Gamma$  valley. When electrons in the central valley have gained energy from the applied electric field which is comparable to the energetic distance between the bottoms of  $\Gamma$  and satellite valleys, the electrons are scattered to the satellite valleys through the longitudinal optical (LO) phonon. The effective mass of electrons in the satellite

valley is considerably heavier than that in central valley; thus, a sudden decrease of drift velocity is expected. Figure 5(b) shows the ideal acceleration of electrons in bulk GaAs when the electrons are in the band as shown in Fig. 5(a). The initial positive part shown in Fig. 5(b) corresponds to the ballistic acceleration of electrons in  $\Gamma$  valley, whereas the subsequent sudden dip corresponds to the deceleration due to intervalley transfer from  $\Gamma$  valley to satellite valleys.

As shown in Fig. 4, the leading edge of the  $E_{\text{THz}}$  observed in the experiment is produced by both the duration of the femtosecond pulses and the limitation of spectral bandwidth of the EO crystal detector. From the experimental data, we can clearly see that the THz emission waveforms have a bipolar feature; i.e., an initial positive peak and a subsequent negative dip that arises from the velocity overshoot<sup>[13]</sup>. The initial positive peak has been interpreted as electron acceleration in  $\Gamma$  valley, where electrons have a light effective mass, whereas the subsequent negative dip has been attributed to electron deceleration due to intervalley transfer from  $\Gamma$  to X and L valleys. From Figs. 4(a) and (b), we can find that at 10 K, the duration time of the waveforms is longer than that at 300 K at any bias electric field,  $F$ . The longer duration of the THz waveforms at 10 K is due to the lower scattering rate of LO phonon at 10 K, which will be discussed in detail in the succeeding sections. Figures 4(a) and (b) also show that  $E_{\text{THz}}$  increases more abruptly with increasing electric field and its bipolar feature becomes pronounced.

Furthermore, we also adhere to the fact that the time domain THz emission experiments inherently measure the step response of electron system to the applied electric field, as described in detail in Ref. [14]. In the THz emission experiment, we set a DC electric field,  $F$ , in the sample and directed a femtosecond laser pulse shot to the sample at  $t = 0$  to create a step-function-like carrier density,  $n\Theta(t)$ . These steps are shown in Figs. 6(a)–(c). Subsequently, THz radiation is emitted due to the accelerated photoexcited electrons (Fig. 6(d)). Based on imagination, we can view the experiment in a different way. Let us perform the following thought experiment, as shown in Figs. 6(e)–(h). We set electrons in the conduction band under a flat band condition (Fig. 6(f)) and

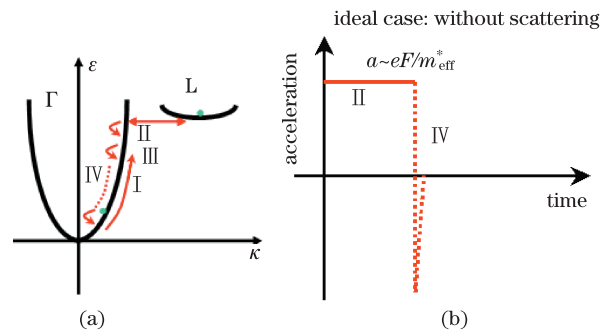


Fig. 5. (a) Band diagram of GaAs. (b) Ideal acceleration of electrons in bulk GaAs. I: acceleration from the bottom of  $\Gamma$  valley; II: intervalley scattering to L valley; III: intervalley scattering back to  $\Gamma$  valley; IV: relaxation to the bottom of  $\Gamma$  valley.

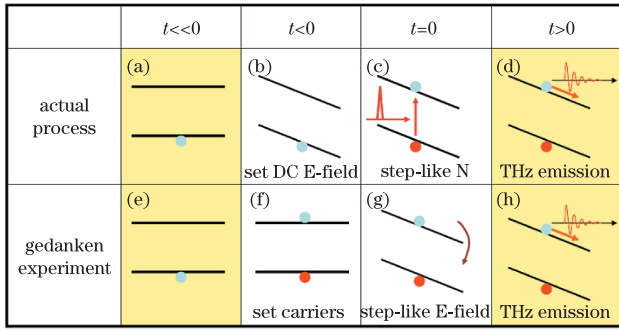


Fig. 6. Comparison between (a)–(d) the real and (e)–(h) thought experiments. Electrons in the thought experiment emit the same THz radiation as in the actual experiment, indicating that time domain THz emission experiments inherently measure the step response of the electron system to the applied electric field.

at  $t = 0$ , and suddenly apply a step-function-like bias electric field,  $F\Theta(t)$  (Fig. 6(g)). Notice that the electrons in the thought experiment emit the same THz radiation in a similar manner as that of the actual experiment (Fig. 6(h)). This indicates that the procedure we performed in our femtosecond laser pulse measurement is equivalent to the application of a step-function-like electric field to electrons. The step-like electric field can be described as

$$F(t) = F_0\Theta(t) = \begin{cases} 0 & (t < 0) \\ F_0 & (t > 0) \end{cases}. \quad (3)$$

By taking note of this important implication, the power dissipation spectra under step-function-like electric fields in the THz range can be obtained from the thought experimental scheme, as shown in the following discussion.

In time domain, the power density is defined as  $P(t) = \frac{\partial \varepsilon}{\partial t} = J(t)F(t)$ , i.e., power density is equal to the product of current density,  $J(t)$ , and electric field,  $F(t)$ . If the direction of  $J(t)$  is the same as that of  $F(t)$ , a Joule heating is produced. However, if  $P(t)$  is negative, a gain is obtained. Similarly, in the frequency domain, if the power dissipation spectrum,  $S(\omega) = \frac{\partial \varepsilon}{\partial \omega}$ , is negative at frequency  $\omega$ , then the system gains energy at this frequency. The power dissipation spectrum,  $S(\omega)$ , is closely related to the differential conductivity spectrum

$$S(\omega) = \sigma(\omega) |F(\omega)|^2, \quad (4)$$

in the linear response regime. However, this formulation, which uses small values of signal conductivity,  $\sigma(\omega)$ , is not strictly correct in a non-linear response situation. Therefore, we should avoid the formulation using  $\sigma(\omega)$  and instead, derive the power dissipation spectrum from our THz-TDS.

Mathematically, the energy,  $\varepsilon$ , can be expressed as

$$\varepsilon = \int_{-\infty}^{+\infty} P(t)dt = V \int_{-\infty}^{+\infty} J(t)F(t)dt, \quad (5)$$

where  $V$  is the volume of sample and  $J(t)$  and  $F(t)$  are the time dependent current density and applied electric

field, respectively. On the other hand,  $\varepsilon$  can also be expressed in the frequency domain as

$$\varepsilon = V \int_{-\infty}^{+\infty} J(t)F(t)dt = \frac{V}{2\pi} \int_{-\infty}^{+\infty} J(\omega)\overline{F}(\omega)d\omega, \quad (6)$$

where  $J(\omega)$  and  $F(\omega)$  are the Fourier spectra of  $J(t)$  and  $F(t)$ , respectively. Subsequently, the power dissipation spectrum is obtained as

$$S(\omega) = \frac{\partial \varepsilon}{\partial \omega} = \frac{V}{2\pi} J(\omega)\overline{F}(\omega). \quad (7)$$

Using simple mathematics,  $J(\omega)$  can be derived from the Fourier transformation of the time domain THz traces as

$$\begin{aligned} J(\omega) &= \int_{-\infty}^{+\infty} J(t) \exp(-i\omega t)dt \\ &\propto \int_{-\infty}^{+\infty} \left[ \int_{-\infty}^t E_{\text{THz}}(t)dt \right] \exp(-i\omega t)dt \\ &= \frac{1}{i\omega} \int_{-\infty}^{+\infty} E_{\text{THz}}(t) \exp(-i\omega t)dt + \pi E_{\text{THz}}(0)\delta(\omega) \\ &= \frac{1}{i\omega} E_{\text{THz}}(\omega) + \pi E_{\text{THz}}(0)\delta(\omega). \end{aligned} \quad (8)$$

As mentioned, the creation of the step-function-like carrier density by the femtosecond laser pulses in the actual experiment can be replaced with the application of step-function-like electric field in the thought experiment scheme. Subsequently,  $F(\omega)$  can be expressed as

$$F(\omega) = \int_{-\infty}^{+\infty} F(t) \exp(-i\omega t)dt = F_0 \left[ \frac{1}{i\omega} + \pi\delta(\omega) \right], \quad (9)$$

where  $F_0$  is the magnitude of the internal electric field applied on the sample.

By simply substituting Eqs. (8) and (9) into Eq. (7), the power dissipation spectrum under step-function-like electric field can be written as

$$S(\omega) = \frac{F_0}{\omega^2} E_{\text{THz}}(\omega) \text{ for } \omega \neq 0. \quad (10)$$

Consequently, we can obtain an important message from Eq. (10): the real and imaginary parts of the Fourier spectra of  $E_{\text{THz}}(t)$  (i.e.,  $\text{Re}[E_{\text{THz}}(\omega)]$  and  $\text{Im}[E_{\text{THz}}(\omega)]$ ) are proportional to  $\text{Re}[S(\omega)]$  and  $\text{Im}[S(\omega)]$ , respectively.

From the above discussion, we realize that from the measured temporal waveforms of THz electric fields emitted from GaAs samples shown in Fig. 4, the power dissipation spectra in the intrinsic bulk GaAs under step-function-like electric fields can be determined by using Fourier transformation of  $E_{\text{THz}}(t)$ . Figures 7(a) and (b) show  $\text{Re}[E_{\text{THz}}(\omega)]$  and  $\text{Im}[E_{\text{THz}}(\omega)]$  for sample #1 under various electric fields at 300 and 10 K, respectively.

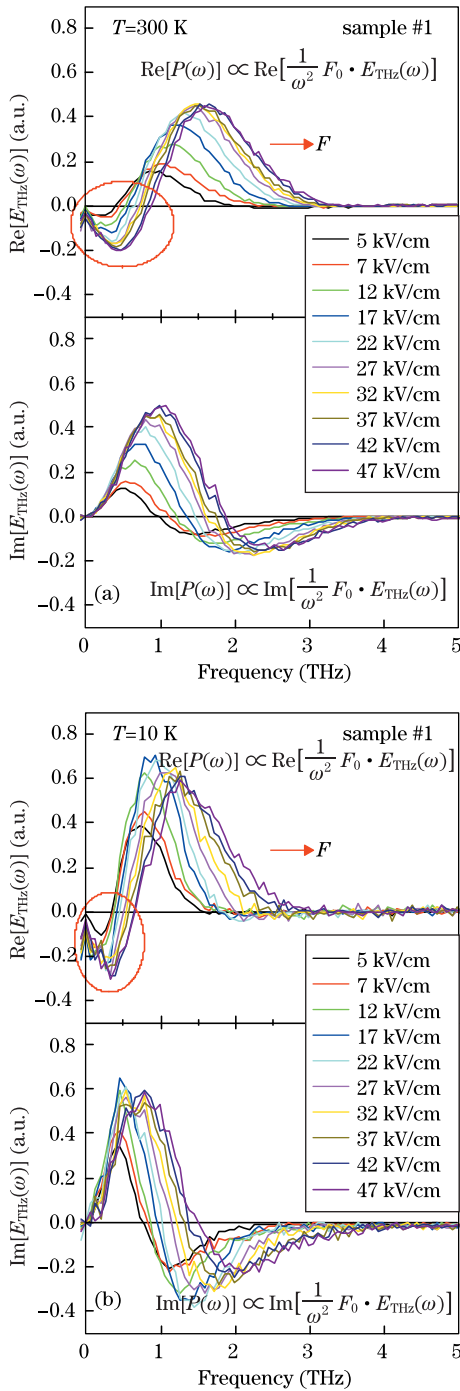


Fig. 7.  $\text{Re}[E_{\text{THz}}(\omega)]$  and  $\text{Im}[E_{\text{THz}}(\omega)]$ , which are proportional to the real and imaginary parts of the power dissipation spectra in bulk GaAs for various values of  $F$  at (a) 300 and (b) 10 K come from the Fourier transformation of THz traces emitted from sample #1.

In  $\text{Re}[E_{\text{THz}}(\omega)]$  plotted in Fig. 7, the negative region of  $\text{Re}[S(\omega)]$  persists up to several hundred gigahertz ( $\sim 800$  GHz at 47 kV/cm at 300 K), indicating that GaAs has an intrinsic gain region up to the THz range. The negative power dissipation turns to positive as the frequency increases. Comparing  $\text{Re}[E_{\text{THz}}(\omega)]$  at 10 and 300 K as shown in Figs. 7(a) and (b), we find that magnitude of  $S(\omega)$  at 10 K is larger and the width is narrower than that at 300 K under the same applied electric fields.

Furthermore, to investigate the power dissipation spec-

tra under extremely large electric fields, we measured the THz-TDS emitted from sample #2 under extremely high electric fields at 300 and 10 K. Figures 8(a) and (b) show the real and imaginary parts of the Fourier spectra of the THz-TDS emitted from sample #2. Even at very high electric fields such as  $F = 300$  kV/cm, the negative  $\text{Re}[E_{\text{THz}}(\omega)]$  still exists at the low frequency region. At high frequency, the  $\text{Re}[E_{\text{THz}}(\omega)]$  changes its sign from negative to positive.

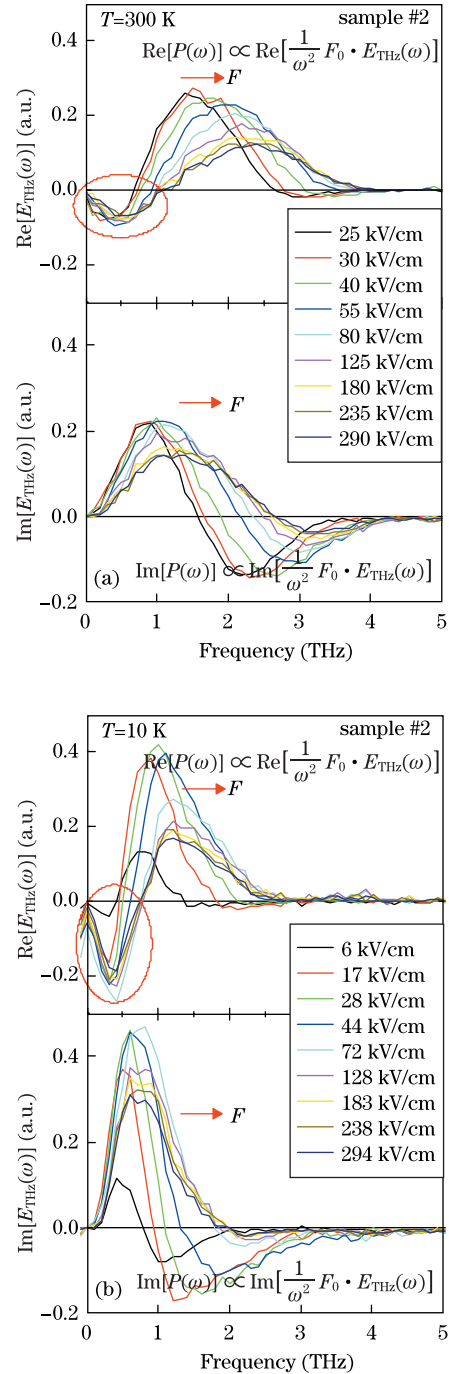


Fig. 8.  $\text{Re}[E_{\text{THz}}(\omega)]$  and  $\text{Im}[E_{\text{THz}}(\omega)]$ , which are proportional to the real and imaginary parts of the power dissipation spectra in bulk GaAs for various values of  $F$  at (a) 300 and (b) 10 K come from the Fourier transformation of THz traces emitted from sample #2.

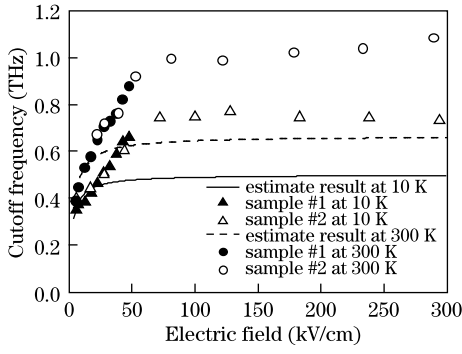


Fig. 9. Cutoff frequencies of the negative region of  $\text{Re}[E_{\text{THz}}(\omega)]$  obtained for sample #1 as a function of the electric field  $F$  at 300 and 10 K are shown by solid circles and triangles, respectively. The open circles and triangles correspond to the cutoff frequencies obtained from sample #2 at 300 and 10 K, respectively. The estimated cutoff frequencies are also plotted as dashed and a solid lines at 300 and 10 K, respectively.

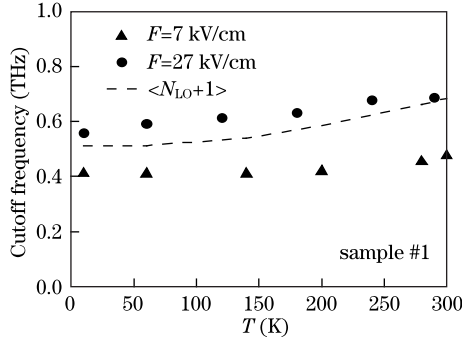


Fig. 10. Cutoff frequencies of the negative region of  $\text{Re}[E_{\text{THz}}(\omega)]$  obtained for sample #1 as a function of temperature at 7 and 27 kV/cm are shown by solid triangles and circles, respectively. The reciprocal of the energy relaxation time due to LO scattering in  $\Gamma$  valley as a function of temperature  $T$  is plotted as a dashed line.

From the real part of the power dissipation spectra, we can derive the cutoff frequencies for the gain region,  $\nu_c$ , at various values of  $F$ . The solid circles and triangles in Fig. 9 show  $\nu_c$  obtained for sample #1 as a function of  $F$  at 300 and 10 K. The open circles and triangles correspond to  $\nu_c$  obtained for sample #2 at 300 and 10 K, respectively. The cutoff frequency increases with increasing  $F$  for  $F < 50$  kV/cm. However, if the value of  $F$  is greater than 50 kV/cm,  $\nu_c$  starts to saturate.

To clarify the mechanism of the cutoff frequency,  $\nu_c$ , we investigated the temperature dependence of  $\nu_c$ . Figure 10 shows the temperature dependence of  $\nu_c$  obtained for sample #1 at 7 and 27 kV/cm as represented by solid triangles and circles, respectively.

In the  $\varepsilon - k$  diagram, the electrons experience a cyclic motion in the  $k$  space; i.e., they become accelerated from the bottom of  $\Gamma$  valley, proceed to L valley by intervalley scattering, are scattered back, and finally relax at the bottom of  $\Gamma$  valley again, as shown in Fig. 5(a).

For this order estimation, we assumed that the electrons are accelerated ballistically by the electric field  $F$  in  $\Gamma$  valley. In addition, we disregarded the acoustic scattering,  $e - e$  scattering. We adhered to the simple New-

ton's law:

$$\frac{\hbar dk}{dt} = -eF, \quad (11)$$

where  $e$  is the elementary charge,  $\hbar = h/2\pi$  where  $h$  is the Planck constant, and  $k$  is the wave vector of electrons. The time for the acceleration process can be estimated by assuming that the energy separation between  $\Gamma$  minimum and the bottom of L valley can be expressed as  $\varepsilon_{\Gamma-L} = 0.29$  eV. The subsequent intervalley scattering time is approximately 50 fs<sup>[26]</sup>.

The energy relaxation process in  $\Gamma$  valley is dominated by LO phonon scattering. Because the LO phonon energy is 36.5 meV, eight LO phonons must be successively emitted in the process. These are required before the electrons from the bottom of L valley can relax upon reaching the bottom of  $\Gamma$  valley ( $\varepsilon_{\Gamma-L} = 0.29$  eV). The relaxation time for one polar scattering process by LO phonon emission in bulk is expressed as<sup>[3]</sup>

$$\begin{aligned} \frac{1}{\tau_{(e)}(\mathbf{k})} &= \frac{2\pi}{\hbar} \frac{1}{(2\pi)^3} \frac{e^2 \hbar \omega_{\text{LO}}}{2\varepsilon_0} \langle N_{\text{LO}} + 1 \rangle \left( \frac{1}{\varepsilon_\infty} - \frac{1}{\varepsilon_s} \right) \\ &\times \frac{m_{\text{eff}}^*}{\hbar^2 \sqrt{|\mathbf{k}'|^2 - \frac{2m_{\text{eff}}^* \hbar \omega_{\text{LO}}}{\hbar^2}}} \times \int_0^{+\infty} \int_0^\pi \int_0^{2\pi} |k'|^2 \sin \theta \\ &\times \frac{1}{|\mathbf{k}' - \mathbf{k}|^2} \delta \left( \left| \mathbf{k}' \right| - \sqrt{|\mathbf{k}|^2 - \frac{2m_{\text{eff}}^* \hbar \omega_{\text{LO}}}{\hbar^2}} \right) d|\mathbf{k}'| d\theta d\varphi, \end{aligned} \quad (12)$$

where  $\varepsilon_0$  is the dielectric permittivity of the vacuum,  $\varepsilon_s$  is the static dielectric constant,  $\varepsilon_\infty$  is the high frequency dielectric constant,  $N_{\text{LO}} = \frac{1}{\exp(\hbar \omega_{\text{LO}}/k_B T) - 1}$  is the thermal equilibrium phonon population per unit volume, which is temperature dependent,  $\hbar = h/2\pi$ , where  $h$  is the Planck constant,  $\omega_{\text{LO}}$  is the frequency of LO phonon,  $m_{\text{eff}}^*$  is the effective mass of electron, and  $\mathbf{k}$  and  $\mathbf{k}'$  are the wave vectors of electrons before and after scattering, respectively. Therefore, we expect the scattering time to be shorter at higher temperatures.

Using Eq. (12), the energy relaxation time in  $\Gamma$  valley was estimated to be 1.46 ps at 300 K and 1.95 ps at 10 K. These were obtained by summing up the emission times of eight LO phonons. The temperature dependence of the energy relaxation time is due to the temperature dependence of the phonon emission process,  $\langle N_{\text{LO}} + 1 \rangle$ . The estimated cutoff frequencies,  $\nu_c$ , at 300 K, are plotted in Fig. 11 where ballistic acceleration are represented by dashed line, intervalley transfer by solid line, energy relaxation by dash-dotted line, and the total by dotted line. Based on this estimation, it is concluded that the energy relaxation process in  $\Gamma$  valley takes the longest time and governs the upper frequency limitation for the gain. Furthermore, the estimated results are plotted in Fig. 9 for comparison with the experimental results. The dashed and straight lines represent the results for 300 and 10 K, respectively. Clearly, the temperature dependence of  $\nu_c$  agrees with that of the emission rate of LO phonons,  $\langle N_{\text{LO}} + 1 \rangle$  (plotted by a dashed line in Fig. 10). The agreement between the experimental results and LO phonon emission rate strongly suggests

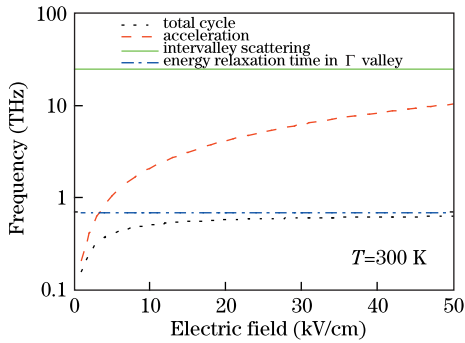


Fig. 11. (Color online) Estimated cutoff frequencies of the negative region of  $\text{Re}[E_{\text{THz}}(\omega)]$  as a function of electric field  $F$  at 300 K are shown as black dashed line. The red dashed line, green solid line, and blue dash-dotted line correspond to the ballistic acceleration, intervalley transfer, and energy relaxation processes in  $\Gamma$  valley at 300 K, respectively.

that  $\nu_c$  is governed by the energy relaxation process of electrons from L to  $\Gamma$  valley via optical phonon emission. At lower temperatures, LO phonon emission rate decreases and a longer energy relaxation time is expected, which results in a lower  $\nu_c$  at 10 K than at 300 K for all the electric fields, as shown in Fig. 9.

In Fig. 9, the overall trend of this estimation of  $\nu_c$  is the same as that of our experimental results. However, at very high electric fields, the magnitude is off by 40%. The discrepancy between the experiment and calculation may have come from the field dependent energy relaxation time of electrons in  $\Gamma$  valley as calculated by Fischetti<sup>[26]</sup>. The calculation results of Fischetti indicate that at very high electric fields, the energy relaxation process is two times faster than that at low electric fields<sup>[26]</sup>. Moreover, the dash-dotted line in Fig. 11 shifts to higher frequency range, which results in higher  $\nu_c$ .

## 4. Conclusion

Taking advantage of the novel experimental method, invaluable information on non-equilibrium carrier transport in the femtosecond time range which is of fundamental interest in semiconductor physics, has been obtained. It should be noted that previously, this has only been discussed through numerical simulations. Furthermore, from the Fourier transformation of the THz-TDS, the power dissipation spectra under step electric field in THz range have also been obtained. The cutoff frequency for the gain is found to gradually increase with increasing electric fields up to 50 kV/cm and saturated at approximately 1 THz at 300 K/750 GHz at 10 K. This gain is governed by the energy relaxation process of electrons from L to  $\Gamma$  valley via successive optical phonon emission. The present insights on the non-stationary carrier transport contribute to a better understanding of device physics in existing high speed electron devices as well as in the process of designing novel ultrafast electromagnetic wave oscillators.

This work was partly supported by the Nano-

technology Special Project of Science and Technology Commission of Shanghai (No. 1052nm07100), the Ministry of Education Doctoral Fund of New Teachers of China (No. 20093120120007), and the National Natural Science Foundation of China (No. 61007059).

## References

1. Y. Yamashita, A. Endoh, K. Shinohara, K. Hikosaka, T. Matsui, S. Hiyamizu, and T. Mimura, *IEEE Electron. Dev. Lett.* **23**, 573 (2002).
2. J. B. Gunn and C. A. Hogarth, *J. Appl. Physics* **26**, 353 (1955).
3. P. J. Bulman, G. S. Hobson, and B. C. Taylor, *Transferred Electron Devices* (Academic Press, London and New York, 1972).
4. P. Das and R. Bharat, *Appl. Phys. Lett.* **11**, 386 (1967).
5. A. F. Gibson, T. W. Granville, and E. G. S. Paige, *J. Phys. Chem. Solid* **19**, 198 (1961).
6. R. Kamoua, H. Eisele, and G. I. Haddad, *Solid State Electron.* **36**, 1547 (1993).
7. M. F. Zybura, S. H. Jones, B. W. Lim, J. D. Crowley, and J. E. Carlstrom, *Solid State Electron.* **39**, 547 (1996).
8. C. Benz and J. Freyer, *Electron. Lett.* **34**, 2351 (1998).
9. Z. Chu, J. Liu, and K. Wang, *Chin. Opt. Lett.* **8**, 697 (2010).
10. L. Miao, D. Zuo, and Z. Jiu, *Chin. Opt. Lett.* **8**, 411 (2010).
11. P. Zhou and D. Fan, *Chin. Opt. Lett.* **9**, 051902 (2011).
12. A. Leitenstrofer, S. Hunsche, J. Shah, M. C. Nuss, and W. H. Knox, *Phys. Rev. Lett.* **82**, 5140 (1999).
13. A. Leitenstrofer, S. Hunsche, J. Shah, M. C. Nuss, and W. H. Knox, *Phys. Rev. B.* **61**, 16642 (2000).
14. Y. Shimada, K. Hiramawa, M. Odnoblioudov, and K. A. Chao, *Phys. Rev. Lett.* **90**, 46806 (2003).
15. Y. M. Zhu, T. Unuma, K. Shibata, and K. Hiramawa, *Appl. Phys. Lett.* **93**, 042116 (2008).
16. Y. M. Zhu, T. Unuma, K. Shibata, and K. Hiramawa, *Appl. Phys. Lett.* **93**, 232102 (2008).
17. Y. M. Zhu, X. X. Jia, L. Chen, D. W. Zhang, Y. S. Huang, B. Y. He, S. L. Zhuang, and K. Hiramawa, *Acta Phys. Sin.* (in Chinese) **58**, 2692 (2009).
18. P. C. M. Planken, H. K. Nienhuys, H. J. Bakker, and T. Wenckeback, *J. Opt. Soc. Am. B* **18**, 313 (2001).
19. Q. Wu and X.-C. Zhang, *Appl. Phys. Lett.* **71**, 1285 (1997).
20. Q. Wu and X.-C. Zhang, *Appl. Phys. Lett.* **70**, 1784 (1997).
21. A. Leitenstorfer, S. Hunsche, J. Shah, M. C. Nuss, and W. H. Knox, *Appl. Phys. Lett.* **74**, 1516 (1999).
22. N. Sekine and K. Hiramawa, *Phys. Rev. Lett.* **94**, 057408 (2005).
23. E. M. Vartiainen, K.-E. Peiponen, and T. Asakura, *Appl. Spectrosc.* **50**, 1283 (1996).
24. E. M. Vartiainen, Y. Ino, R. Shimano, M. Kuwata-Gonokami, Y. P. Svirko, and K.-E. Peiponen, *J. Appl. Phys.* **96**, 4171 (2004).
25. E. Gornov, E. M. Vartiainen, and K.-E. Peiponen, *Appl. Opt.* **45**, 6519 (2006).
26. M. V. Fischetti, *IEEE Trans. Electron. Dev.* **38**, 634 (1991).